Absence of coupled thermal interfaces in $Al_2O_3/Ni/Al_2O_3$ sandwich structure

Xiangyu Li,[1,2] Wonjun Park,[1,3] Yong P. Chen,[1,3,4] and Xiulin Ruan[1,2,a)]
[1]*Birck Nanotechnology Center, West Lafayette, Indiana 47907, USA*
[2]*School of Mechanical Engineering, Purdue University, West Lafayette, Indiana 47907, USA*
[3]*School of Electrical and Computer Engineering, Purdue University, West Lafayette, Indiana 47907, USA*
[4]*Department of Physics and Astronomy, Purdue University, West Lafayette, Indiana 47907, USA*

(Received 30 April 2017; accepted 19 September 2017; published online 2 October 2017)

Sandwich structures of aluminum oxide, nickel, and aluminum oxide films are fabricated by atomic layer deposition to study thermal interfacial resistance between a metal and a dielectric material and the interfacial coupling effect across a thin metal layer. Thermal resistance of a thin nickel layer as well as two interfaces is measured using the 3ω method. Experimental results show interfacial resistance between nickel and aluminum oxide to be $6.8 \times 10^{-3} mm^2\,K/W$ at 300 K, with a weak dependence on the metal thickness and temperature. A two-temperature model and a detailed diffuse mismatch model have been used to estimate interfacial resistance theoretically, and the results agree reasonably well with experiments. Estimations from the two temperature model indicate that in the overall thermal interfacial resistance, the phonon-phonon interfacial resistance dominates over the resistance due to the electron-phonon coupling effect and inside the metal layer. Also, the phonon-phonon interfacial resistance does not vary as the metal layer thickness decreases below the electron-phonon cooling length, indicating that the two adjacent interfaces are not thermally coupled. *Published by AIP Publishing*. https://doi.org/10.1063/1.5006174

As the thickness of thin films in integrated circuits decreases, the interfacial resistance between metals and dielectric components[1] ($\sim 10^{-2}\,mm^2\,K/W$) becomes comparable to or even larger than the thermal resistance of thin films ($\sim$10 nm). Due to different main carriers of thermal energy in dielectric and metals, electron-phonon non-equilibrium occurs near interfaces. However, it has been shown that when the metal layer thickness decreases to be comparable to the phonon mean free path, phonons can transport through the metal layer,[2] while electrons do not participate much in thermal transport. Furthermore, in nanostructures with a higher interface density and minimal lattice mismatch, coherent phonons are also found to decrease the total thermal resistance.[3–6] Similarly, the cooling length is also studied as the length where electrons and phonons reach equilibrium for metal-dielectric interfaces.[7] For a sandwich structure with a metal layer in the middle, the metal layer is responsible for electron-phonon coupling of two interfaces. A shorter metal thickness than the cooling length also interferes with the electron-phonon coupling effect. Both findings indicate that interfaces are no longer isolated but dependent on the thickness of the thin film that separates them. The first finding is studied both theoretically and experimentally. The second one, however, needs more work.

In this work, we use the differential 3ω method to measure the interfacial resistance of a thin nickel layer sandwiched between two aluminum oxide layers, with the nickel layer thickness varying from 10 nm, 15 nm to 30 nm. The temperature dependence of the interfacial resistance is also studied. The two temperature model and diffuse mismatch model (DMM) are used to calculate the theoretical interfacial resistance, which agrees reasonably well with experimental values. Overall, thermal resistance is dominated by phonon mismatch resistance. Since phonon mismatch resistance does not vary even when the metal layer thickness decreases around the cooling length, the two adjacent interfaces in our sandwich structures are not thermally coupled even as the nickel layer falls below the electron cooling length.

We have fabricated two sandwich structures in this work to measure the interfacial resistance between nickel and aluminum oxide, illustrated in Fig. 1. Schematic views are shown along with TEM images (Transmission Electron Microscope). Before film depositions, silicon wafers were cleaned using the RCA method (the Radio Corporation of America), and any residues or silicon oxide layer on the surface were removed by dipping in HF (Hydrogen Fluoride). Both aluminum oxide and nickel layers are deposited using atomic layer deposition (ALD) to ensure the smooth interfaces and consistent thickness. On sample A, the reference sample, a 40 nm aluminum oxide layer is deposited on the silicon substrate. For samples B and C with the Ni layer, a 20 nm aluminum oxide layer is deposited followed by a thin layer of nickel and then another 20 nm aluminum oxide layer. The aluminum oxide layer is deposited at 250 °C with a rate of 0.12 nm/cycle, and the nickel layer at 250 °C with a rate of 0.2 A/cycle with the thickness varying from 10 nm, 15 nm, to 30 nm. A layer of Pt is deposited on the structures during FIB (Focused Ion Beam) lift-off, only intended for TEM images.

For thin film and interfacial resistance measurements, the time-domain thermoreflectance (TDTR) method[8] and the differential 3ω method[9–11] are widely applied. Both methods yield reliable results.[12] The formal one shines a pulsed heating laser as well as a weaker probe laser on the metal surface. By monitoring the transient thermal response of these ultrashort pulses, interfacial resistance is obtained. The differential 3ω method measures the total thermal resistance difference between the thin film sample and the reference

a)E-mail: ruan@purdue.edu

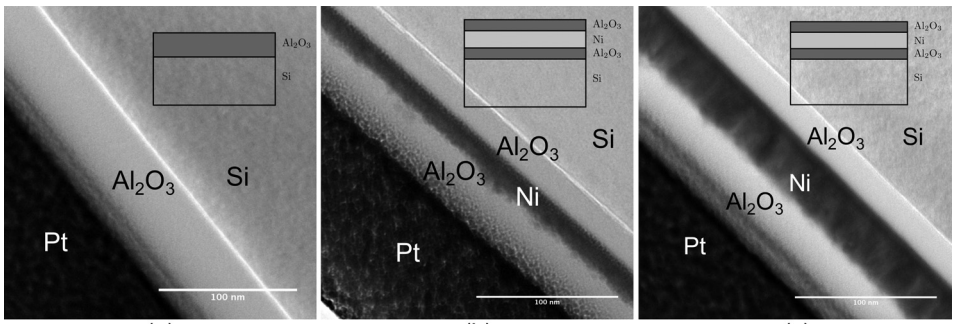

FIG. 1. Sandwich structures in our work for the thermal interfacial resistance measurement. (a) Sample A, 40 nm alumina on silicon. (b) Sample B, 10 nm Ni layer inserted. (c) Sample C, 30 nm Ni layer inserted.

sample to obtain interfacial resistance. However, temperature control of TDTR is more difficult compared to the 3ω method, as the pulsed heating laser has the tendency to excite electrons in the surface metal film rapidly.

In this work, we apply the differential 3ω method. The Ti/Au metal line of 3 mm long and 30 μm wide is later patterned by photolithography for the 3ω measurement. An AC current of frequency ω is applied to the metal line, resulting in a temperature oscillation amplitude ΔT and a voltage of 3ω frequency. Three lock-in amplifiers are utilized to monitor metal line $v_{1\omega}$, $v_{3\omega}$, and power consumption p. For a bulk sample, ΔT can be expressed as

$$\Delta T = \frac{2v_{3\omega}}{v_{1\omega}C_{rt}} = \frac{p}{\pi k}\int_0^\infty \frac{\sin^2(\lambda b)}{(\lambda b)^2(\lambda^2 + 2i\omega/D)^{1/2}}d\lambda, \quad (1)$$

where p is the power consumption across the metal line, k and D are the thermal conductivity and thermal diffusivity of the sample, b is the half width of the metal line, and $v_{1\omega}$ and $v_{3\omega}$ are the voltage across the metal line with frequencies ω and 3ω, respectively. In this work, the samples A and B are measured separately, leading to different temperature oscillations and total thermal resistance difference ΔR[11] as

$$\Delta R = 2bl\left(\left(\frac{\Delta T}{p}\right)_B - \left(\frac{\Delta T}{p}\right)_A\right) = R_{Ni} + 2R_i \approx 2R_i, \quad (2)$$

where R_i stands for interfacial resistance between nickel and alumina, which is about half of the total thermal resistance difference measured by the 3ω method. Uncertainties evaluated as $(\Delta T/p)_{R+F} - (\Delta T/p)_R$ at different frequencies are collected regarding Eq. (2), which produce most uncertainties. Uncertainties are valued in a similar fashion for thickness-dependent and temperature dependent thermal conductivity.

To study the potential interface coupling effect when the thickness of the middle metal thin film is comparable to twice the electron-phonon cooling length, the interfacial resistance is measured as a function of different nickel layer thicknesses. When the metal layer is thinner than or comparable to the phonon mean free path, long-wavelength coherent phonons will travel ballistically through two interfaces as one coupled interface, rather than experiencing two interfaces separately, resulting in lower overall thermal resistance.[3] This is how interfaces become coupled due to ballistic transfer of phonons. If the nickel film is much thicker than most of the phonons' mean free path, most phonons will travel across two interfaces separately. The cooling length stands for the electron-phonon non-equilibrium distance.[7] As the metal layer connects two metal-dielectric interfaces, electron-phonon coupling is affected once the metal layer is thinner than twice the cooling length, resulting in thickness-dependent interfacial resistance. Considering that the mean free path for nickel is around 5 nm and the cooling length is around 15 nm, the nickel layer thickness is chosen as 10 nm, 15 nm, and 30 nm, and the interfacial resistance is $6.7\pm0.6 \times 10^{-3}$ mm^2 K/W, $6.7\pm0.8 \times 10^{-3}$ mm^2 K/W, and $7.0\pm0.7 \times 10^{-3}$ mm^2 K/W, respectively. The results from the 3ω measurement are shown in Fig. 2.

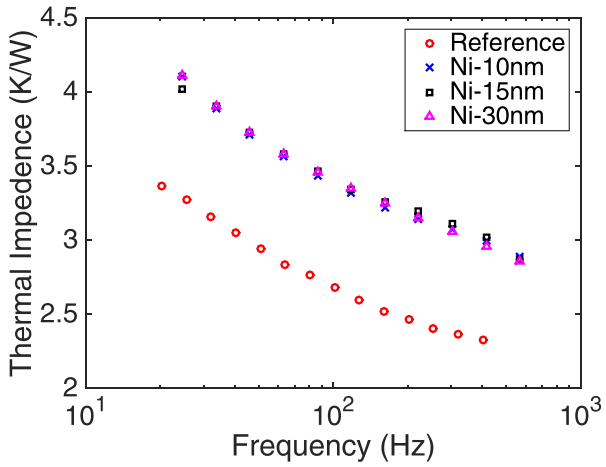

FIG. 2. Characterization of the thickness-dependent thermal interface resistance using the differential 3ω method.

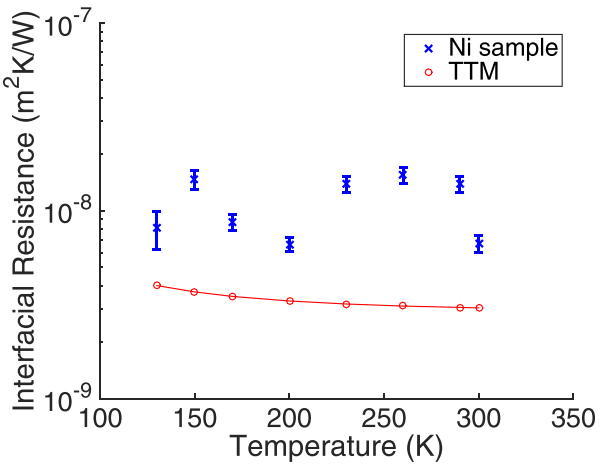

FIG. 3. Temperature dependence of the thermal interfacial resistance measured using the differential 3ω method, compared with TTM results.

The temperature dependence of the interfacial resistance is taken using liquid nitrogen to provide the temperature as low as 130 K. The result is shown in Fig. 3, indicating that the interfacial resistance does not depend much on temperature changes either.

Due to differences in main heat carriers, electrons and phonons at different sides of the interface between the metal and dielectric materials may have a large difference in kinetic energy, when the electron-phonon coupling effect could be significant.[2,13] It is more reasonable to combine both the electron-phonon coupling effects with the phonon mismatch model than to apply either of them alone. Electron inelastic scattering across the interface is also possible for materials with high electron density. The two-temperature model[7,13–18] is a simple approach to implement the electron-phonon coupling effect by assuming two different temperatures for phonons and electrons separately across the interface.

The overall interfacial resistance consists of a phonon-phonon scattering resistance R_{pp}, an electron-phonon coupling component R_{ep}, electrical inelastic scattering resistance R_{ei}, and phonon transport channel inside the metal layer R_p, as shown in Fig. 4.[19] R_{pp} is the thermal interface resistance when phonons travel across the interface. Compared to phonons in the nickel film, electrons are more efficient in heat transfer, and thus, most energy is transferred to nickel electrons through electron-phonon coupling component R_{ep}. R_e is the thermal resistance for nickel electrons. For thermal energy remained in nickel phonons, R_p is the thermal resistance for phonons across the nickel film. On the other hand, R_{ei} stands for the process where electrons in alumina transfer energy directly to nickel electrons without participations of any phonons. Because of the low density of electrons in aluminum oxide, R_{ei} is neglected in this work.

Compared to the acoustic mismatch model (AMM)[20,21] which works on ideal interfaces, the diffuse mismatch model (DMM)[21] is more suitable in this case for modeling the phonon scattering term R_{pp} as grain boundaries in the nickel layer shown in Fig. 1 are visible. Certain modifications[22] are proposed for high temperatures, by introducing and relying on parameters fitted with experimental data, although the use of such fitting parameters may take the agreement coincidental. By assuming that phonons lose their memories and randomize directions across the interface, DMM utilizes the detailed balance as $\alpha_{A\to B} = \alpha_{B\to A}$ to calculate transmission coefficient $\alpha_{A\to B}$ and thermal interfacial conductance $h_{A\to B}$ as

$$\alpha_{A\to B}(\omega') = \frac{\sum_j DOS_{B,j}(\omega)v_{B,j}(\omega)\delta_{\omega',\omega}}{\sum_j DOS_{A,j}(\omega)v_{A,j}(\omega)\delta_{\omega',\omega} + \sum_j DOS_{B,j}(\omega)v_{B,j}(\omega)\delta_{\omega',\omega}}, \tag{3}$$

$$h_{A\to B} = \frac{1}{4}\sum_j \int \hbar\omega DOS_{A,j} v_{A,j}\alpha_{A\to B}\frac{\partial f}{\partial T}d\omega, \tag{4}$$

where h is the thermal interfacial conductance, $\hbar$ is reduced Planck's constant, $DOS_{A,j}$ is the phonon density of state of mode j and material A, v is the phonon group velocity, f is the Bose-Einstein distribution function, and δ is the Kronecker delta function. From these two equations, we are able to calculate thermal interface resistance based on DMM with phonon dispersions, known by lattice dynamics, shown in Fig. 5. Only acoustic phonon branches of aluminum oxide are considered since the frequencies of nickel phonons have little overlap with other phonon branches in aluminum oxide and thus a negligible transmission coefficient. It should be noted that nickel is polycrystalline and aluminum oxide is amorphous in experiments due to the fabrication process, while in lattice dynamics, we assume the crystallized structure for simplification. Regarding the electron-phonon coupling effect, two different temperatures assigned for electrons and phonons are coupled as

$$\begin{aligned} k_e\frac{\partial^2 T_e}{\partial z^2} - G_{ep}(T_e - T_p) = 0, \\ k_p\frac{\partial^2 T_p}{\partial z^2} + G_{ep}(T_e - T_p) = 0, \end{aligned} \tag{5}$$

where G_{ep} is the electron-phonon coupling factor for the metal material,[15,23] k_e is the electron thermal conductivity,

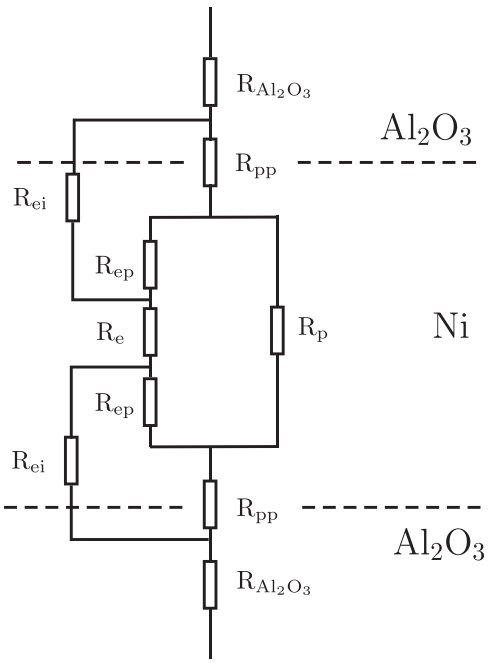

FIG. 4. Thermal resistance network between nickel and aluminum oxide.

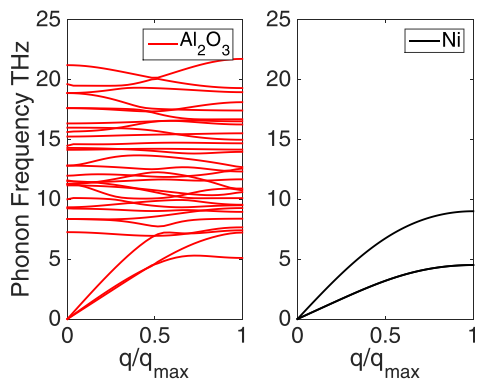

FIG. 5. Detailed phonon dispersion of aluminum oxide and nickel.

and k_p is the lattice thermal conductivity of the metal, calculated using non-equilibrium molecular dynamics (NEMD).[24,25] G_{ep} is chosen as the bulk value for the electron-phonon coupling factor. It is reported to consist of the bulk and surface electron-phonon coupling component, with the former one varying with the thin film thickness below the mean free path of phonons.[26–28] However, quantitative estimation of G_{ep} in the range of 10 nm to 30 nm still needs additional work in further studies. In our work, because of the low contribution of electron-phonon coupling to total thermal interface resistance, only the bulk coupling factor is applied. With further mathematical deductions,[7] R_{ep} can be calculated as

$$R_{ep} = \left(\frac{k_e}{k_e + k_p}\right)^{3/2} \left(\frac{1}{G_{ep} k_p}\right)^{1/2}. \quad (6)$$

Direct phonon transfer within the nickel layer R_p can be approximated as d/k_p, where d is the thickness of the nickel layer. For nickel,[25] k_p is 5.5 W/mK for the 10 nm film, 6.4 W/mK for the 15 nm film, 8.9 W/mK for the 30 nm film, and 18 W/mK for bulk nickel. On the other hand, k_e remains around 40 to 60 W/mK for 10 nm to 30 nm nickel films.[29] The total thermal interfacial resistance R_i is calculated as

$$R_i = R_{pp} + R_{ep} // \frac{R_p}{2} = R_{pp} + \frac{R_p R_{ep}}{R_p + 2R_{ep}}. \quad (7)$$

The theoretical values together with the experimental values are listed in Table I. First, the phonon transmission resistance component dominates the overall thermal interfacial resistance due to the highly lattice mismatch between nickel and aluminum oxide. On the other hand, R_p increases with the increasing metal layer thickness, while R_{ep} decreases. The combination of R_p and R_{ep} indicates the possible highest resistance between the 10 nm and 30 nm nickel layer. However, it is still much smaller and less important than phonon mismatch resistance to have a high impact.

With the temperature changing from 130 K to 300 K, the electron-phonon coupling coefficient G_{ep} decreases from 2.88×10^{17} W m^{-3} K^{-1} at 300 K to 5.62×10^{17} W m^{-3} K^{-1} at 130 K. However, interfacial resistance barely changes, both theoretically and experimentally. Since the Debye temperature of nickel is relatively low at 450 K and aluminum oxide at 873 K, the temperature range of 130 K to 300 K is not sufficient to observe temperature dependent phonon transmission resistance. Thus, as the dominant phonon mismatch resistance is not sensitive to temperature, the overall estimated interface resistance remains almost constant even if G_{ep} changes significantly.

In conclusion, we fabricated sandwich structures of nickel and Al_2O_3 and used the differential 3ω method to measure interfacial thermal resistance. Theoretical estimation is also made using the two temperature model along with detailed DMM. The overall interfacial resistance from experiments agrees reasonably well with theoretical prediction. Phonon mismatch is still the dominating mechanism for the interfaces between nickel and aluminum oxide. Interfaces remain independent even when the thickness of the metal layer decreases to the electron-phonon cooling length.

TABLE I. Interfacial resistance with different Ni thicknesses.

Ni layer (nm)	$R_p/2$	R_{ep}	$R_{ep} // \frac{R_p}{2}$	R_{pp}	$R_{i,theo}$	$R_{i,exp}$
10	0.91[a]	0.79	0.42	3.04	3.46	6.7
15	1.67	0.74	0.51	3.04	3.55	6.7
30	1.69	0.63	0.46	3.04	3.50	7.0

[a]Interfacial resistance unit as 10^{-3} mm^2 W/K.

[1]R. J. Stevens, A. N. Smith, and P. M. Norris, "Measurement of thermal boundary conductance of a series of metal-dielectric interfaces by the transient thermoreflectance technique," J. Heat Transfer **127**, 315 (2005).
[2]E. Dechaumphai, D. Lu, J. J. Kan, J. Moon, E. E. Fullerton, Z. Liu, and R. Chen, "Ultralow thermal conductivity of multilayers with highly dissimilar Debye temperatures," Nano Lett. **14**, 2448–2455 (2014).
[3]M. N. Luckyanova, J. Garg, K. Esfarjani, A. Jandl, M. T. Bulsara, A. J. Schmidt, A. J. Minnich, S. Chen, M. S. Dresselhaus, Z. Ren, E. A. Fitzgerald, and G. Chen, "Coherent phonon heat conduction in superlattices," Science **338**, 936–939 (2012).
[4]J. Ravichandran, A. K. Yadav, R. Cheaito, P. B. Rossen, A. Soukiassian, S. J. Suresha, J. C. Duda, B. M. Foley, C.-H. Lee, Y. Zhu, A. W. Lichtenberger, J. E. Moore, D. A. Muller, D. G. Schlom, P. E. Hopkins, A. Majumdar, R. Ramesh, and M. A. Zurbuchen, "Crossover from incoherent to coherent phonon scattering in epitaxial oxide superlattices," Nat. Mater. **13**, 168–172 (2014).
[5]Y. Wang, H. Huang, and X. Ruan, "Decomposition of coherent and incoherent phonon conduction in superlattices and random multilayers," Phys. Rev. B **90**, 165406 (2014).
[6]J. Shi, Y. Dong, T. Fisher, and X. Ruan, "Thermal transport across carbon nanotube-graphene covalent and van der Waals junctions," J. Appl. Phys. **118**, 044302 (2015).
[7]Y. Wang, X. Ruan, and A. K. Roy, "Two-temperature nonequilibrium molecular dynamics simulation of thermal transport across metal-nonmetal interfaces," Phys. Rev. B **85**, 205311 (2012).
[8]D. G. Cahill, W. K. Ford, K. E. Goodson, G. D. Mahan, A. Majumdar, H. J. Maris, R. Merlin, and S. R. Phillpot, "Nanoscale thermal transport," J. Appl. Phys. **93**, 793 (2003).
[9]D. G. Cahill, "Thermal conductivity measurement from 30 to 750 K: The 3ω method," Rev. Sci. Instrum. **61**, 802 (1990).
[10]D. G. Cahill, "Thermal conductivity of thin films: Measurements and understanding," J. Vac. Sci. Technol. A: Vac., Surf., Films **7**, 1259 (1989).
[11]T. Borca-Tasciuc, A. R. Kumar, and G. Chen, "Data reduction in 3ω method for thin-film thermal conductivity determination," Rev. Sci. Instrum. **72**, 2139 (2001).
[12]Y. K. Koh, S. L. Singer, W. Kim, J. M. O. Zide, H. Lu, D. G. Cahill, A. Majumdar, and A. C. Gossard, "Comparison of the 3ω method and time-domain thermoreflectance for measurements of the cross-plane thermal conductivity of epitaxial semiconductors," J. Appl. Phys. **105**, 054303 (2009).
[13]A. Majumdar and P. Reddy, "Role of electronphonon coupling in thermal conductance of metal nonmetal interfaces," Appl. Phys. Lett. **84**, 4768 (2004).
[14]D. M. Duffy and A. M. Rutherford, "Including the effects of electronic stopping and electronion interactions in radiation damage simulations," J. Phys.: Condens. Matter **19**, 16207 (2007).
[15]Z. Lin, L. Zhigilei, and V. Celli, "Electron-phonon coupling and electron heat capacity of metals under conditions of strong electron-phonon nonequilibrium," Phys. Rev. B **77**, 075133 (2008).
[16]L. Koči, E. M. Bringa, D. S. Ivanov, J. Hawreliak, J. McNaney, A. Higginbotham, L. V. Zhigilei, A. B. Belonoshko, B. A. Remington, and R. Ahuja, "Simulation of shock-induced melting of Ni using molecular dynamics coupled to a two-temperature model," Phys. Rev. B **74**, 012101 (2006).
[17]R. E. Jones, J. A. Templeton, G. J. Wagner, D. Olmsted, and N. A. Modine, "Electron transport enhanced molecular dynamics for metals and semi-metals," Int. J. Numer. Methods Eng. **83**, 940–967 (2010).
[18]Z. Lu, Y. Wang, and X. Ruan, "Metal/dielectric thermal interfacial transport considering cross-interface electron-phonon coupling: Theory, two-temperature molecular dynamics, and thermal circuit," Phys. Rev. B - Condens. Matter Mater. Phys. **93**, 064302 (2016).
[19]Z. Li, S. Tan, E. Bozorg-Grayeli, T. Kodama, M. Asheghi, G. Delgado, M. Panzer, A. Pokrovsky, D. Wack, and K. E. Goodson, "Phonon dominated heat conduction normal to Mo/Si multilayers with period below 10 nm," Nano Lett. **12**, 3121–3126 (2012).

[20]W. A. Little, "The transport of heat between dissimilar solids at low temperatures," Can. J. Phys. **37**, 334–349 (1959).
[21]E. Swartz and R. Pohl, "Thermal boundary resistance," Rev. Mod. Phys. **61**, 605–668 (1989).
[22]R. S. Prasher and P. E. Phelan, "A scattering-mediated acoustic mismatch model for the prediction of thermal boundary resistance," J. Heat Transfer **123**, 105 (2001).
[23]C. L. Phillips and P. S. Crozier, "An energy-conserving two-temperature model of radiation damage in single-component and binary Lennard-Jones crystals," J. Chem. Phys. **131**, 074701 (2009).
[24]R. E. Jones, J. C. Duda, X. W. Zhou, C. J. Kimmer, and P. E. Hopkins, "Investigation of size and electronic effects on Kapitza conductance with non-equilibrium molecular dynamics," Appl. Phys. Lett. **102**, 183119 (2013).
[25]P. Heino and E. Ristolainen, "Thermal conduction at the nanoscale in some metals by MD," Microelectron. J. **34**, 773–777 (2003).
[26]H. Fan, B. Zou, Y. Liu, and S. Xie, "Size effect on the electron-phonon coupling in CuO nanocrystals," Nanotechnology **17**, 1099–1103 (2006).
[27]J. A. Sobota, S.-L. Yang, D. Leuenberger, A. F. Kemper, J. G. Analytis, I. R. Fisher, P. S. Kirchmann, T. P. Devereaux, and Z.-X. Shen, "Distinguishing bulk and surface electron-phonon coupling in the topological insulator Bi_2Se_3 using time-resolved photoemission spectroscopy," Phys. Rev. Lett. **113**, 157401 (2014).
[28]M. Maier, M. Schätzel, G. Wrigge, M. Astruc Hoffmann, P. Didier, and B. V. Issendorff, "Bulk-like electron-phonon coupling in small free sodium clusters," Int. J. Mass Spectrom. **252**, 157–165 (2006).
[29]Y. Shiping and J. Peixue, "Thermal conductivity of nanoscale thin nickel films," Prog. Nat. Sci. **15**, 922–929 (2005).